Supplementary material

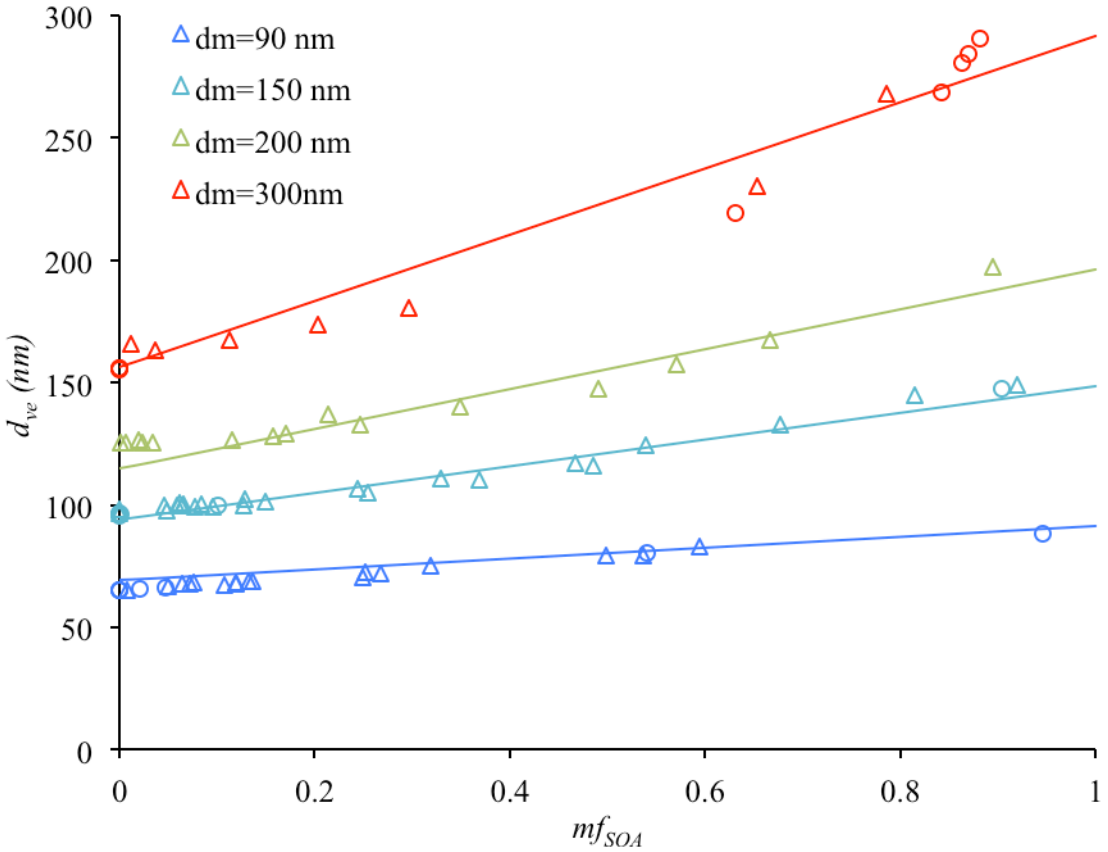

Figure S 1. Empirically derived volume equivalent diameters (d_{ve}) for mobility diameters (d_m) of 90 nm (red), 150 nm (green), 200 nm (purple) and 300 nm (blue). Diesel exhausts particles (DEP1, 2 and 3, triangles) as well as flame soot particles (FSP1, circles) with a primary particle diameter (d_{pp}) of 28 nm are used for the fitting. The estimated d_{ve} (lines) is calculated from measured d_m and the SOA mass fraction (mf_{SOA}) of the particles (see Eq. (11) and (12) in Sect.5.3).

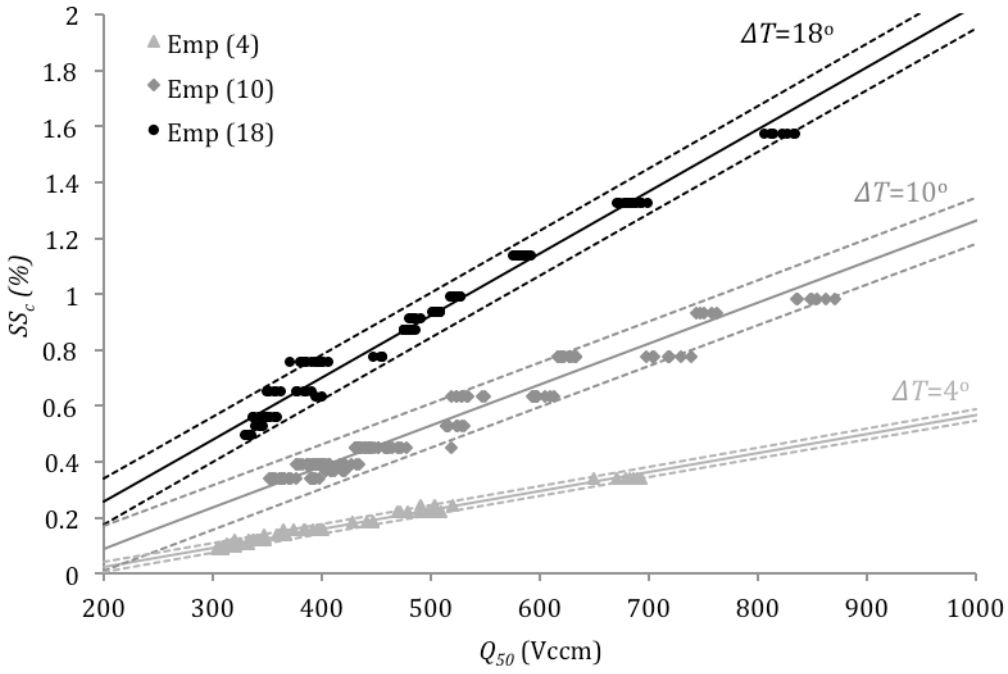

Figure S 2. Illustration of calibration measurements performed with AS (for ΔT=4, 10 and 18 K) and sucrose (ΔT=18 K) for one of the CCNC. Measured values (markers) and the corresponding fit (lines) with 95% confidence intervals (dotted lines) for the three different ΔT used in the study. The slope and intercept of the 18 K line are 0.00221984 and -0.1882434; the slope and intercept for the 10 K are 0.00146469 and -0.2063209; and for the 4 K the slope and intercept are 0.00067888 and -0.1128603.

ADCHAM model simulations of the DEP2 experiment

Here we describe how the ADCHAM model (Roldin et al., 2014) was used to simulate the gas-phase chemistry, secondary organic aerosol (SOA) formation and its properties during the DEP2 experiment. For the model simulations it is assumed that the gas-phase chemistry in the chamber is primarily driven by the NO_x emissions from the Euro II Diesel Passenger Vehicle, the added light-aromatic precursors (toluene and m-xylene), and the alkene, alkyne and aldehyde emissions from the diesel vehicle. The absolute alkene, alkyne and aldehyde concentrations in the chamber (c_i) (Table S1), are estimated by scaling their concentrations reported by Schauer et al. (1999) ($c_{i,Schauer}$) with our measurements of light-aromatic compounds (C6-C9) from the DEP4 experiment (Eq. (S1)).

$$c_i = c_{i,Schauer} \cdot \frac{[\text{light-arom.}]_{\text{DEP4}}}{[\text{light-arom.}]_{\text{Schauer}}} \quad \text{(S 1)}$$

Table S 1. Estimated initial alkene, alkyne and aldehyde concentrations in the Teflon chamber during the DEP2 and DEP4 experiments.

	c_i (ppbv)
Alkenes	
Ethene	13.03
Propene	0.79
Trans-2-butene	0.20
Cis-2-butene	0.40
Isobutene	0.87
3-methyl-1-butene	0.10
2-methyl-1-butene	0.16
1,3-butadiene	0.24
Total	**15.79**
Alkynes	
Ethyne	7.54
Aldehydes	

Formaldehyde	31.68
Acetaldehyde	40.48
Propanal	10.29
Total	**82.45**

Gas-phase chemistry

In the model the simulations start with estimated concentrations of alkene, alkyne and aldehyde (Table S1) and the measured initial NO and NO_2 concentration of 420 and 150 ppb, respectively. Between 20 and 90 minutes after the input of diesel vehicle emissions O_3 are slowly added (~5.3 ppb/min) to the modelled chamber in order to capture the conversion of NO to NO_2 prior to the onset of the UV-light (see Fig. S3a). 30 minutes before the UV-lights are turned on 430 ppb of toluene and 310 ppb of *m*-xylene are added to the chamber. Unfortunately the toluene and *m*-xylene concentrations were not measured during the DEP2 experiment. Thus, the concentrations were estimated based on the GC-MS measurements during the DEP4 experiment, in which the same amount of toluene and *m*-xylene were injected. The gas-phase chemistry in the chamber was modelled with the kinetic mechanism from Master Chemical Mechanism v3.2 (MCMv3.2; Jenkin et al., 2003; Bloss et al., 2005a and b), including all compounds in Table S1, toluene, *m*-xylene and all inorganic reactions (in total 772 compounds and 2446 reactions). Bloss et al. (2005a and b) have shown that the MCMv3.1 generally overestimates the ozone concentration and underestimates the OH concentration during oxidation of light aromatic compounds (e.g. xylene and toluene). Similar model and measurement discrepancy was also observed by Roldin et al. (2014) when simulating the photooxidation of *m*-xylene in the 6 m^3 Teflon chamber used in the present study. In order to improve the model performance Bloss *et al.* (2005b) and Roldin *et al.* (2014) included an artificial OH source after the UV-lights are turned on. In this work the same artificial OH source rate are used as in Roldin *et al.* (2014) of 10^8 cm^{-3} s^{-1}. With the artificial OH source the model better captures the observed temporal evolution of the NO and O_3 concentrations.

Chamber wall effects

The ADCHAM model explicitly treats the deposition of particles and gases onto the Teflon walls, the mass transfer limited diffusion of gases across a thin laminar layer (Δx) adjacent to the Teflon walls, and the mass transfer of organic compounds to and from the particles deposited on the chamber walls. Table S2 list the values used for different model parameters related to the mass transfer to and from the Teflon walls. See Roldin et al. (2014) for detailed information about how all these parameters are used in ADCHAM. The parameter values were adopted from Roldin et al. (2014) in which ADCHAM was used to simulate the SOA formation during a *m*-xylene experiment in the Teflon chamber in the Aerosol Laboratory at Lund University.

Table S 2. Parameters used to calculate the chamber wall effects in ADCHAM.

Parameter	Description	Value (unit)
V_0	Initial chamber volume	5.95 (m^3)
$\Delta V / \Delta t$	Volume loss rate in chamber	-0.4# (m^3 h^{-1})
V_t	Chamber volume at time t	$V_0 + \Delta V / \Delta t \cdot t$
$\bar{E}$	Mean electrical field strength	$50 \cdot V_0 / V_t$ (V cm^{-1})
u^*	Friction velocity	0.25#, 0.05#** (m s^{-1})
$k_{g,w}$	First order loss rate from the near wall gas phase to the walls	1/15 (s^{-1})
$k_{w,g}$	Desorption rate from the chamber wall Teflon surfaces	$k_{w,g,i} = \frac{k_{g,w}}{(RT / p_{0,i} C_w / (M_w \gamma_{w,i})}$ (s^{-1})
$C_{w,i}$	Effective wall equivalent mass concentration of compound *i*	(mol m^{-3})
M_w	Average molar mass of the Teflon film	(mol)
$\gamma_{w,i}$	Activity coefficient of compound *i* in the Teflon film	
$p_{0,i}$	Pure liquid saturation vapour pressure of compound *i*	(Pa)
$C_w / (M_w \gamma_{w,i})$	Measureable parameter, for uptake on Teflon walls (see Matsunaga	100 (μmol m^{-3})***

	and Ziemann, 2010)	
Δx	Laminar layer adjacent to the Teflon walls	10^{-3} (m)
E_{HONO}	HONO wall emissions during photooxidation	4.6×10^{8} molecules cm^{-2} s^{-1}

[#]Different value than used by Roldin et al. (2014).
**Value used before the UV-light are turned on.
***The same value was used for all condensable organic compounds

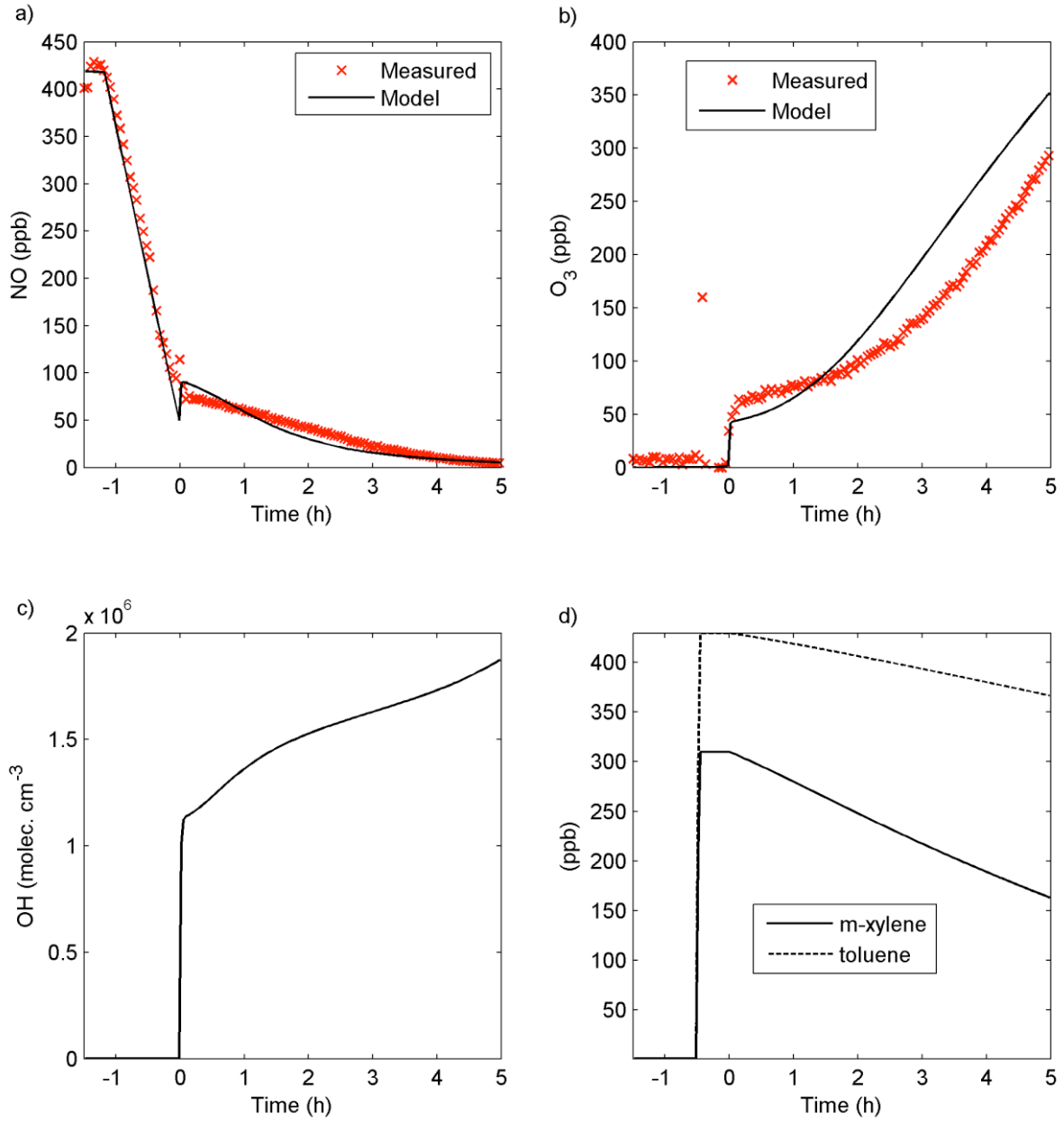

Figure S 3. Modelled (a) NO(g), (b) O_3(g), (c) OH(g) and (d) *m*-xylene(g) and toluene(g) concentrations for the DEP2 experiment. In (a) and (b) the modelled concentrations can be compared with the measured. The UV onset is at time 0 h in the figures.

Particle-phase chemistry and SOA formation

Oxidation products from the added light-aromatic precursors m-xylene and toluene dominate the SOA formed during the DEP2 experiment. However a small fraction of the SOA is also originating from other organic compounds present in the diesel exhausts (e.g. *n*-alkanes and PAHs).

The SOA formation from *m*-xylene and toluene are modelled by considering the non-equilibrium gas-particle partitioning of all their non-radical oxidation products in MCMv3.2. In Roldin et al. (2014) it was shown that ADCHAM could not capture the observed early stage SOA formation during an *m*-xylene oxidation experiment, if not considering particle-phase oligomerization. However, with peroxyhemiacetal (aldehydes + hydroperoxides) and hemiacetal (alcoholes + aldehydes) dimer formation rates (k_f) of 10^{-22} cm^3 s^{-1}, ADCHAM were able to nearly reproduce the temporal evolution of the SOA concentration during the complete oxidation experiment (~4 hours). Here we will test to simulate the SOA formation both with and without these particle-phase oligomerization processes.

In order to account for the SOA formation from known PAHs and *n*-alkanes measured in diesel exhausts, we use the measurements from Schauer et al. (1999). Eq. (S1) is used for estimating the absolute *n*-alkane and PAH concentrations in the chamber. Table S3 gives the estimated initial PAH and *n*-alkane concentrations, and their first order reaction rate with OH radicals ($k_{OH,i}$).

Table S 3. Estimated initial PAH and *n*-alkane concentrations in the Teflon chamber during the DEP2 and DEP4 experiments, and $k_{OH,i}$ used in the model simulations.

	c_i (ppbv)	$k_{OH,i}$ (cm^3 $molec^{-1}$ s^{-1})
PAHs		
Naphthalene	0.2054	$2.3x10^{-11}$ (a)
2-methylnaphthalene	0.1860	$4.86x10^{-11}$ (b)
1-methylnaphthalene	0.1151	$4.09x10^{-11}$ (b)
C2-naphthalene	0.1520	$6.0x10^{-11}$ (c)
C3-naphthalene	0.0624	$8.0x10^{-11}$ (d)
C4-naphthalene	0.0236	$8.0x10^{-11}$ (d)

other PAHs	0.2010	8.0×10^{-11} [d]
Total	**0.9453**	
n-alkanes		
Dodecane	0.1276	1.32×10^{-11} [a]
Tridecane	0.1117	1.51×10^{-11} [a]
Tetradecane	0.1368	1.79×10^{-11} [a]
Pentadecane	0.0808	2.07×10^{-11} [a]
Hexadecane	0.1353	2.32×10^{-11} [a]
Heptadecane	0.1099	2.85×10^{-11} [e]
Octadecane	0.1016	3.51×10^{-11} [e]
Nonadecane	0.0658	4.32×10^{-11} [e]
Eicosane	0.0414	5.31×10^{-11} [e]
Total	**0.9108**	

[a] Atkinson and Arey (2003)
[b] Phousongphouang and Arey (2002)
[c] Average of all dimethylnaphthalanes in Phousongphouang and Arey (2002)
[d] Estimated from dimethylnaphthalenes, assumed to be same for all other PAHs according to Chan et al. (2009)
[e] Estimated from structure-reactivity relationships (Kwok and Atkinson, 1995)

The SOA formation from the PAHs were modelled with the one or two product SOA yield parameterizations from Chan et al. (2009), for high-NO_x conditions. For the n-alkanes we estimate the SOA yields based on the modelling from Jordan et al. (2008), using a 1-product model parameterization (Eq. (S2)),

$$Y_i = M_o \frac{\alpha_i K_i}{1 + K_i M_o} \quad \text{(S 2)}$$

where α_i is the mass-based stoichiometric yield of the oxidation product i, K_i is its gas-particle partitioning equilibrium constant, and M_o is the total particulate organic mass concentration.

Table S 4. Estimated mass-based stoichiometric yields (α_i), equilibrium partitioning constants (K_i) and pure liquid saturation vapour pressures ($p_{0,i}$), derived from the SOA yield parameterizations of different n-alkanes (Eq. (S2)).

c_i	α_i	K_i (m^3 μg^{-1})	$p_{0,i}$ (Pa)
Dodecane	0.0472	0.0489	2.109×10^{-4}
Tridecane	0.0898	0.0333	2.925×10^{-4}
Tetradecane	0.1536	0.0320	2.883×10^{-4}

Pentadecane	0.2775	0.0272	3.221×10^{-4}
Hexadecane	0.3531	0.0341	2.447×10^{-4}
Heptadecane	0.4402	0.0554	1.437×10^{-4}
Octadecane	0.5430	0.0823	9.25×10^{-5}
Nonadecane	0.6280	0.1350	5.41×10^{-5}
Eicosane	0.7837	0.1668	4.20×10^{-5}

ADCHAM includes a kinetic multilayer model, which considers the diffusion of compounds between different particle layers. For the model simulations performed here each particle is treated as composed of one solid soot core, one amorphous organic bulk phase layer and one particle surface monolayer, with limited diffusion between the layers. The aerosol dynamic processes considered are: Brownian coagulation, condensation/evaporation and dry deposition to the chamber walls. For more details see Roldin et al. (2014).

Before the onset of UV radiation in the chamber a substantial increase of the O:C ratio from ~0.05 to ~0.2 is observed, meanwhile the H:C ratio decreases from ~1.9 to ~1.75 (see Fig. S4d). However, no particle mass increase or change in the mass spectra is observed during this time, other than a slight increase in m/z 44 due to CO_2^+. According to the ADCHAM model simulations there were very low concentrations of NO_3 radicals ($<10^6$ molecules cm^{-3}), OH (<3000 molecules cm^{-3}) and O_3 (<1 ppbv), before the UV-light was turned on. Hence, the change in O:C and H:C ratio during the dark conditions is unlikely attributed to SOA formation. Instead it can be explained by heterogeneous oxidation of POA with NO_2, which reaches a maximum concentration of ~500 ppb, just before the onset of the UV-lights. The heterogeneous oxidation of diesel soot coated with POA has previously primarily been studied because of the potential importance for HONO formation (e.g. Arens et al., 2001; Han et al., 2013).

For the simulations presented here it is assumed that the POA is composed of slightly oxidized *n*-alkanes, and alkenes with an average number of carbon atoms per molecule of 26, two carbon-carbon double bonds, and one ketone functional group (H:C=1.8846, O:C=0.0385). The POA are assumed to react with NO_2 with a reaction rate (k_{NO_2}) equal to 10^{-18} cm^{-3} s^{-1}, forming oxidized POA (OPOA) with an H:C of 1.6538 and O:C of 0.1923. The uptake of NO_2 is modelled with the kinetic multilayer model, considering the adsorption and diffusion of NO_2 between the surface monolayer and the organic bulk phase, analogous to Roldin et al. (2014). The NO_2 diffusion coefficient was assumed to be equal to 10^{-8} cm^2 s^{-1}.

Figure S4 shows the modelled and measured: (a) particle number concentration, (b) total organic particle mass concentration in the air, (c) organic mass fraction (mf_{OA}) and (d) H:C and O:C ratios. When accounting for deposition of charged and neutral particles two the

chamber walls, according to the procedure described in Roldin et al. (2014) (although with five times larger friction velocity) and Brownian coagulation, the modelled particle number concentrations are in good agreement with the observations. The model performance substantially improves if we consider hemiacetal and peroxyhemiacetal (oligomer) formation. However, in contrast to the *m*-xylene experiment in Roldin et al. (2014), ADCHAM still substantially underestimates the total organic particle mass and mf_{OA} (SOA formation) 0-2 hour after the UV exposure starts.

Figure S5 shows the temporal evolution of the modelled mass concentration of POA, OPOA and SOA formed from oxidation products of light-aromatic compounds (*m*-xylene and toluene), *n*-alkanes and PAHs. According to the model results the mass contribution from *n*-alkane oxidation products are negligible, and the contribution from the considered PAHs (Table S2) are ~4 times too small to explain the observed early stage SOA formation. This indicates that we either substantially underestimates the PAH concentrations in the chamber or that there are some unknown IVOCs in the Diesel exhausts which we do not account for. Another possibility could also be that we cannot realistically represent the early stage SOA formation from the *m*-xylene and toluene oxidation products. Possibly, a reactive uptake mechanism not directly driven by the oxidation products saturation vapour pressures but their reactivity with other organic compounds on the particle surfaces, could explain the almost immediate onset of the SOA formation, after the UV-light is turned on. However, this is not fully consistent with the *m*-xylene experiment simulated in Roldin et al. (2014), or other classical photooxidation experiments of light-aromatic compounds (see e.g. Ng et al., 2007). Figure S6 shows the measured and modelled total organic particle mass plotted against the amount of reacted *m*-xylene and toluene (Δm-xylene + Δtoluene). According to the model simulations ~120 μg/m^3 of *m*-xylene and ~40 μg/m^3 of toluene have been consumed before the OA mass starts to increase in the air. However from the measurements in combination with the modelled *m*-xylene and toluene decay, only ~30 μg/m^3 of *m*-xylene and ~10 μg/m^3 of toluene need to react before the OA mass increases.

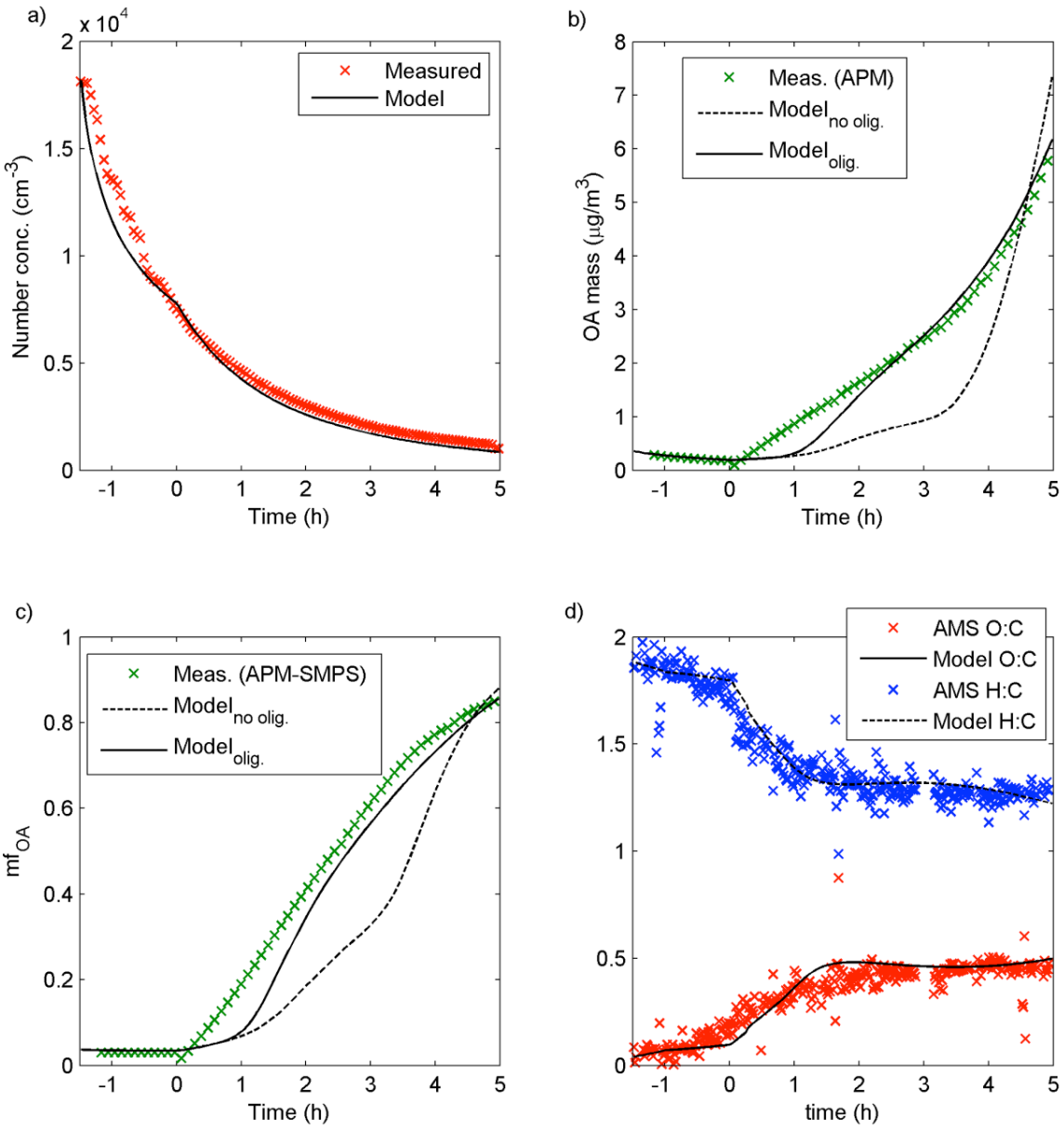

Figure S 4. Modelled and measured (a) particle number concentration, (b) OA mass, (c) mf_{OA} and (d) H:C and O:C ratios for the DEP2 experiment. The onset of UV exposure is at time 0 h in the figures. In (b) and (c) the model results from simulations with (solid line) and without (dashed line) particle phase oligomerization are included. In (a) and (d) the results are from the simulation with oligomerization.

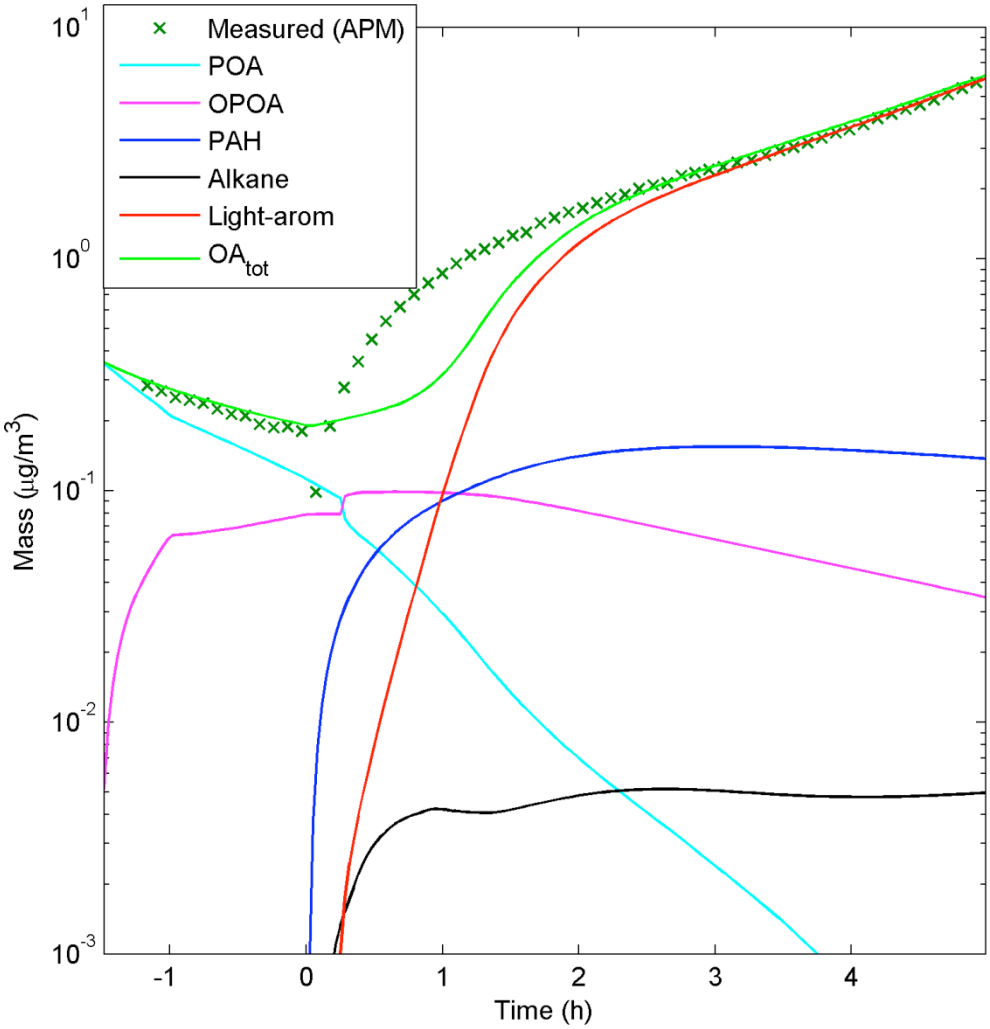

Figure S 5. Modelled (lines) and measured (markers; APM-SMPS) total organic particle mass (in the air) for the DEP2 experiment. Given are also the modelled POA (turquoise), OPOA (pink) formed from the heterogeneous reactions between POA and NO_2, and SOA originating from the light-aromatic precursors (m-xylene and toluene) (red), PAHs (blue) and *n*-alkanes (black). We have also included the modelled total organic mass (light green) in the air and on the wall deposited particles. At time 0 h in the figure the UV-lights are turned on.

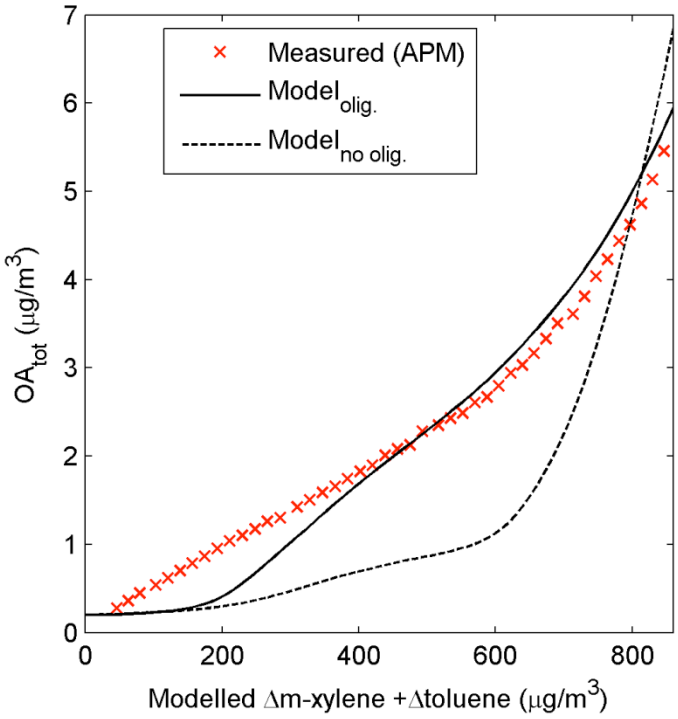

Figure S 6. Measured (APM) and modelled total organic particle mass concentration (OA_{tot}) plotted against the amount of reacted *m*-xylene and toluene.

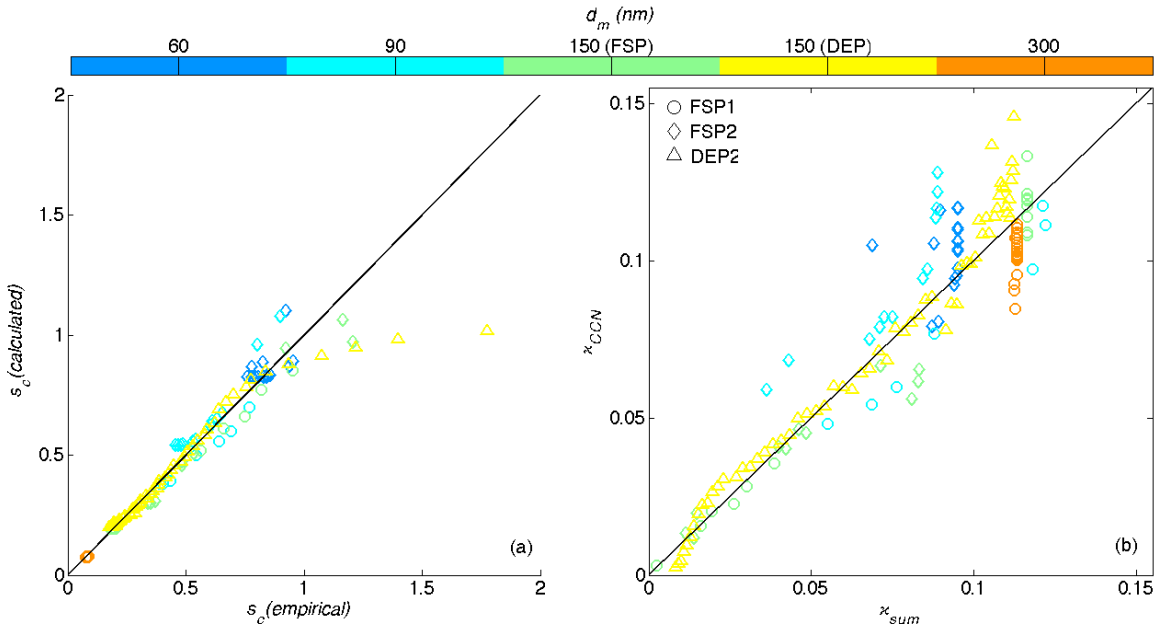

Figure S 7. Comparison of calculated s_c and empirical results (a) and comparison of κ_{SOA} with κ_{CCN} (b), calculated from the chemical composition and measured s_c respectively. The large

discrepancies for the high values of s_c in (a) are due to the under prediction of the s_c by the model of the early aged soot particles. Small values in (b) correspond to modelled and measured values (κ_{SOA} and κ_{CCN}) for early aged soot particles, where uncertainties are large for κ_{CCN}. For large values in (b) the uncertainties are inherited from empirical fitting of the mf_{SOA} (visible for FSP1; d_m =150 and 300 nm, and for FSP2; d_m=60 and 90 nm.)

Determining mf_{OA} from the SP-AMS data

Quantification by means of AMS is a two-step process. First, the signal is assigned to species (such as 'organics', 'rBC' etc., see next paragraph), using the fragmentation table approach (Allan et al., 2004). Then, a species is quantified using two parameters: collection efficiency (CE) and ionization efficiency (IE) (Allan et al., 2004). CE refers to the fraction of the mass that is eligible for ionization, normally dominated by bounce of the tungsten vaporizer (Huffman *et al.*, 2005). For PM vaporized by the SP-module, the main issue is overlap of particle and laser beams. IE is the probability that ionization occurs, decoupled from CE (i.e. given that the material is not bouncing of the tungsten vaporizer, missing the laser beam etc.) Since ammonium nitrate is the default calibration substance, IEs are often expressed in terms of relative ionization efficiencies compared to nitrate.

Refractory Black Carbon (rBC) mass loadings were estimated assuming a relative ionization efficiency (compared to nitrate) of 0.2, applied to the $C_{1\text{-}9}^+$ ions (signal due to $C_{>9}$ was negligible) after accounting for the organic contribution to C_1^+ (the contribution to $C_{2\text{-}9}^+$ was negligible). C_1^+ was apportioned to rBC as 70% of C_3^+, (C_3^+ was chosen because it is the most abundant) the remaining signal from C_1^+ was interpreted as organic. This was based on measurements on fresh soot in each experiment, where the organic contribution to C_1^+ was negligible. rBC also generated CO_2^+ ions (and presumably CO^+, but these were not retrieved owing to the interference from N_2^+), these were found to correspond to 70-90% of C_3^+. These CO_2^+ ions where excluded from the results presented here, pending further investigation. A CE of 1 was applied for both organics and rBC.

Determining mf_{OA} from combined DMA-APM and SMPS measurements

The total organic mass fraction of the polydisperse particle size distribution was determined from a procedure that started with determining the mass size distribution by multiplying the measured number size distribution from the SMPS with the size resolved mass per particle determined with the DMA-APM. This mass size distribution was then divided into a volatile

(organic) and a non-volatile fraction by, in a size resolved manner, multiplying the mass distribution with the volatile mass fraction for each size bin. The DMA-TD-APM measured in the size range 60 to 300 nm at five discrete mobility sizes. Data at other sizes were obtained by fitting a physically relevant function.

Corresponding atmospheric ageing timescales

The modelled cumulative OH exposure during the end of the DEP2 experiment is 7.7×10^6 cm^{-3} h. This together with the measured mass spectral signature of the organic material (see Sec.5.2) illustrate that, with respect to chemical composition, the SOA during the experiment is relatively fresh (a few hours of ageing for typical summer daytime conditions). Still, for mid-latitude winter conditions this cumulative OH exposure may very well correspond to one or a few days in the atmosphere.

In the smog chamber experiments the SOA precursor concentration is substantially higher than for typical atmospheric conditions, while the condensation sinks of the diesel soot particles, are comparable with typical urban plume conditions (see e.g. Roldin et al., 2011). Hence, substantially higher mass growth rates are expected in the chamber compared to typical atmospheric urban plume conditions. To some extent this is counteracted by the uptake of condensable organic compounds onto the Teflon walls and wall deposited particles.

In the smog chamber the time of photochemical ageing, before the soot particles become CCN active at a supersaturation of 0.2%, range from 1.5 to >4.5 h depending on experimental conditions as well as particle size. To estimate the corresponding atmospheric ageing time the range of observed new particle growth rates (GR) in the mid-latitudes of 1-20nm/h has been used (Kulmala et al., 2004). It is also assumed that these growth rates (if converted to mass growth rates) are valid for soot particles with a mobility diameter (d_m) of ~100 nm (volume equivalent diameter ($d_{ve,fresh}$) of ~70 nm). According to the experiments these particles need to have an mf_{SOA} of ~90 % before they activate at a supersaturation of 0.2% (see Figure 11). At this stage these particles have a volume equivalent diameter ($d_{ve,\mathrm{aged}}$) equalling the mobility diameter (d_m) of ~150 nm, i.e. the particles are almost spherical. Hence, based on this the atmospheric ageing time with respect to organic condensational growth (t_{atm}) is estimated to be between 4 hours and 3 days (Eq. (S3)).

$$t_{atm} = \frac{\left(d_{ve,\text{aged}} - d_{ve,fresh}\right)}{GR} \qquad \text{(S 3)}$$

References Supplementary

Allan, J. D., Delia, A. E., Coe, H., Bower, K. N., Alfarra, M. R., Jimenez, J. L., Middlebrook, A. M., Drewnick, F., Onasch, T. B., Canagaratna, M. R., Jayne, J. T. and Worsnop, D. R. "A generalised method for the extraction of chemically resolved mass spectra from aerodyne aerosol mass spectrometer data." [In English]. Journal of Aerosol Science 35, no. 7 (Jul 2004): 909-922.

Arens, F., Gutzwiller, L., Baltensperger, U., Gaggeler, H. W. and Ammann, M. "Heterogeneous reaction of NO2 on diesel soot particles." [In English]. Environmental Science & Technology 35, no. 11 (Jun 1 2001): 2191-2199.

Atkinson, R. and Arey, J. "Atmospheric degradation of volatile organic compounds." [In English]. Chemical Reviews 103, no. 12 (Dec 2003): 4605-4638.

Bloss, C., Wagner, V., Bonzanini, A., Jenkin, M. E., Wirtz, K., Martin-Reviejo, M. and Pilling, M. J. "Evaluation of detailed aromatic mechanisms (MCMv3 and MCMv3.1) against environmental chamber data." [In English]. Atmospheric Chemistry and Physics 5 (Mar 1 2005a): 623-639.

Bloss, C., Wagner, V., Jenkin, M. E., Volkamer, R., Bloss, W. J., Lee, J. D., Heard, D. E., Wirtz, K., Martin-Reviejo, M., Rea, G., Wenger, J. C. and Pilling, M. J. "Development of a detailed chemical mechanism (MCMv3.1) for the atmospheric oxidation of aromatic hydrocarbons." [In English]. Atmospheric Chemistry and Physics 5 (Mar 1 2005b): 641-664.

Chan, A. W. H., Kautzman, K. E., Chhabra, P. S., Surratt, J. D., Chan, M. N., Crounse, J. D., Kurten, A., Wennberg, P. O., Flagan, R. C. and Seinfeld, J. H. "Secondary organic aerosol formation from photooxidation of naphthalene and alkylnaphthalenes: implications for oxidation of intermediate volatility organic compounds (IVOCs)." [In English]. Atmospheric Chemistry and Physics 9, no. 9 (2009): 3049-3060.

Han, C., Liu, Y. C. and He, H. "Role of Organic Carbon in Heterogeneous Reaction of NO2 with Soot." [In English]. Environmental Science & Technology 47, no. 7 (Apr 2 2013): 3174-3181.

Huffman, J. A., Jayne, J. T., Drewnick, F., Aiken, A. C., Onasch, T., Worsnop, D. R. and Jimenez, J. L. "Design, modeling, optimization, and experimental tests of a particle beam width probe for the aerodyne aerosol mass spectrometer." [In English]. Aerosol Science and Technology 39, no. 12 (Dec 2005): 1143-1163.

Jenkin, M. E., Saunders, S. M., Wagner, V. and Pilling, M. J. "Protocol for the development of the Master Chemical Mechanism, MCM v3 (Part B): tropospheric degradation of aromatic

volatile organic compounds." [In English]. Atmospheric Chemistry and Physics 3 (Feb 12 2003): 181-193.

Jordan, C. E., Ziemann, P. J., Griffin, R. J., Lim, Y. B., Atkinson, R. and Arey, J. "Modeling SOA formation from OH reactions with C-8-C-17 n-alkanes." [In English]. Atmospheric Environment 42, no. 34 (Nov 2008): 8015-8026.

Kroll, J. H., Donahue, N. M., Jimenez, J. L., Kessler, S. H., Canagaratna, M. R., Wilson, K. R., Altieri, K. E., Mazzoleni, L. R., Wozniak, A. S., Bluhm, H., Mysak, E. R., Smith, J. D., Kolb, C. E. and Worsnop, D. R. "Carbon oxidation state as a metric for describing the chemistry of atmospheric organic aerosol." [In English]. Nature Chemistry 3, no. 2 (Feb 2011): 133-139.

Kulmala, M., Vehkamaki, H., Petaja, T., Dal Maso, M., Lauri, A., Kerminen, V. M., Birmili, W. and McMurry, P. H. "Formation and growth rates of ultrafine atmospheric particles: a review of observations." [In English]. Journal of Aerosol Science 35, no. 2 (Feb 2004): 143-176.

Kwok, E. S. C. and Atkinson, R. "Estimation of Hydroxyl Radical Reaction-Rate Constants for Gas-Phase Organic-Compounds Using a Structure-Reactivity Relationship - an Update." [In English]. Atmospheric Environment 29, no. 14 (Jul 1995): 1685-1695.

Matsunaga, A. and Ziemann, P. J. "Gas-Wall Partitioning of Organic Compounds in a Teflon Film Chamber and Potential Effects on Reaction Product and Aerosol Yield Measurements." [In English]. Aerosol Science and Technology 44, no. 10 (2010): 881-892.

Ng, N. L., Kroll, J. H., Chan, A. W. H., Chhabra, P. S., Flagan, R. C. and Seinfeld, J. H. "Secondary organic aerosol formation from m-xylene, toluene, and benzene." [In English]. Atmospheric Chemistry and Physics 7, no. 14 (2007): 3909-3922.

Phousongphouang, P. T. and Arey, J. "Rate constants for the gas-phase reactions of a series of alkylnaphthalenes with the OH radical." [In English]. Environmental Science & Technology 36, no. 9 (May 1 2002): 1947-1952.

Rissler, J., Messing, M. E., Malik, A. I., Nilsson, P. T., Nordin, E. Z., Bohgard, M., Sanati, M. and Pagels, J. H. "Effective Density Characterization of Soot Agglomerates from Various Sources and Comparison to Aggregation Theory." [In English]. Aerosol Science and Technology 47, no. 7 (Jul 1 2013): 792-805.

Roldin, P., Eriksson, A. C., Nordin, E. Z., Hermansson, E., Mogensen, D., Rusanen, A., Boy, M., Swietlicki, E., Svenningsson, B., Zelenyuk, A. and Pagels, J. "Modelling non-equilibrium secondary organic aerosol formation and evaporation with the aerosol dynamics, gas- and particle-phase chemistry kinetic multi-layer model ADCHAM." Atmos. Chem. Phys. Discuss 14 (2014): 769-869.

Roldin, P., Swietlicki, E., Massling, A., Kristensson, A., Londahl, J. L., Eriksson, A., Pagels, J. and Gustafsson, S. "Aerosol ageing in an urban plume - implication for climate." [In English]. Atmospheric Chemistry and Physics 11, no. 12 (2011): 5897-5915.

Schauer, J. J., Kleeman, M. J., Cass, G. R. and Simoneit, B. R. T. "Measurement of emissions from air pollution sources. 2. C-1 through C-30 organic compounds from medium duty diesel

trucks." [In English]. Environmental Science & Technology 33, no. 10 (May 15 1999): 1578-1587.